CHEMISTRY OF MATERIALS
Article

Chem. Mater. **2009,** *21,* 5711–5718 5711
DOI:10.1021/cm901896g

Holographic Recording with Polymer Nanocomposites Containing Silver Nanoparticles Photogenerated in Situ by the Interference Pattern

Lavinia Balan,*[,†] Colette Turck,[†] Olivier Soppera,[†] Loïc Vidal,[‡] and Daniel J. Lougnot[†]

[†]*Département de Photochimie Générale (CNRS-FRE3252), Université de Haute-Alsace, 3 rue Alfred Werner, 68093 Mulhouse, France and* [‡]*Institut de Science des Matériaux de Mulhouse LRC 7228, 15 rue Jean Starcky, 68093 Mulhouse, France*

Received June 30, 2009. Revised Manuscript Received October 30, 2009

A process allowing in situ photochemically assisted synthesis of silver nanoparticles (NPs) in a polymerizable acrylic formulation was developed and the photopolymerization of this formulation was studied. It has been found that the presence of NPs does not perturb the polymerization process in the least, making it possible to fabricate metal/polymer nanocomposites by a one-step, one-pot photochemical process. The size distribution of NPs was very narrow and their size could be controlled by the chemical parameters of the reactive formulation. This system was used to record holographic gratings, and it was observed that both the holographic sensitivity and the diffraction efficiency at maximum were significantly improved in the presence of particles. Moreover, AFM analysis revealed a clear-cut segregation of photochemically generated NPs between dark and bright regions of the incident pattern, thus demonstrating the possibility to manipulate nascent particles with light gradients.

1. Introduction

Because of the increasing demand for practicable use of photopolymers in holographic data storage[1] and other photonics applications,[2] a wide variety of novel materials have been introduced to achieve larger refractive changes or improved dimensional stability. The optical properties of metal nanoparticules embedded in a polymer matrix have been a subject of immense interest in recent years because of their novel characteristics and possible device applications.[3] In most of these investigations, nanoparticles plasmon resonance has been shown to be the major cause for the change in optical absorption behavior as a function of the metal particle size. This local field enhancement perturbs both linear and nonlinear optical transitions, which induces a lot of consequences: enhancement of fluorescence,[4] two-photon excitation factor,[5] Raman scattering,[6] and change of the radiative characteristics of the excited singlet states.[7] All these properties can be turned to account for the development of innovative applications such as apertureless microscopies, surface-enhanced Raman spectroscopy (SERS), or radiative decay engineering.

The development of periodically ordered metal structures opens up new vistas because of the possibility to couple propagative lightwave and surface plasmons, a promising field of research and development for designing diffractive optical elements with ultrahigh spectral dispersion.[8]

As regards holographic materials for storage applications, the introduction of an additional neutral component within the reactive formulation is a recurring concern for those who are developing new recording systems. It is based on the counterdiffusion of the components of the holographic formulation between the bright and dark regions under the influence of gradients of chemical potential induced by the photopolymerization of monomers. In the search for more and more innovative systems, Vaia et al. pioneered the use of nanoparticles (inorganics, organic polymers, metals or metal oxides).[9] High diffraction efficiencies were reported in polymerizable blends containing NPs (metals or oxides) synthesized beforehand.[10] However, dispersing the nanoparticles in the reactive formulation was always mentioned as a critical step in the process.

*Corresponding author. Tel.: +33 389 335 016. Fax: +33 389 335 014. E-mail: lavinia.balan@uha.fr.

(1) (a) Sheridan, J. T.; Gleeson, M. R.; Close, C. E.; Sabol, D. *Proc. SPIE* **2007**, *6698*, 669807–669807-13. (b) Haw, M. *Nature* **2003**, *422*, 556. (c) Park, J.; Kim, E. *Key Eng. Mater.* **2005**, *277*−*279*, 1039.
(2) (a) Suzuki, N.; Tomita, Y. *Appl. Phys. Lett.* **2006**, *88*(1), 011105. (b) Campbell, M.; Scharp, K. N.; Harrison, M. T.; Denning, R. G.; Tuberfield, A. J. *Nature* **2000**, *404*, 53.
(3) Bronstein, L. M.; Valetsky, P.; Antonietti, M. In *Nanoparticles and Nanostructures Films. Preparation, Characterization and Applications*; Fendler, J. Ed.; Wiley-VCH: Weinheim, Germany, 1998.
(4) Sokolov, K.; Chumanov, G.; Cotton, T. *Anal. Chem.* **1998**, *70*, 3998.
(5) Shalaev, V. M. In *Non Linear Optics of Random Media*; Springer Tracts in Modern Physics; Springer: Berlin, 2000.
(6) Chang, R. K.; Furtak, T. A. *Surface-Enhanced Raman Scattering*; Plenum: New York, 1982.
(7) Lakowicz, J. R. *Ann. Biochem.* **2001**, *298*, 1.
(8) Mikhailov, V.; Eliott, J.; Wurtz, G.; Bayvel, P.; Zayats, A. V. *Phys. Rev. Lett.* **2007**, *99*, 83901.
(9) Vaia, R. A.; Dennis, C. L.; Natarajian, L. V.; Tondiglia, V. P.; Tomlin, D. W.; Bunning, T. J. *Adv. Mater.* **2001**, *23*, 1570.
(10) (a) Nakamura, T.; Nozaki, J.; Tomita, Y.; Ohmori, K; Hidaka, M. *J Opt. A: Pure Appl. Opt.* **2009**, *11*(2), 024010–1. (b) Sanchez, C.; Escuti, M.; Heesh, C.; Bastiaansen, C.; Broer, D.; Loos, J.; Nussbaumer, R. *Adv. Funct. Mater.* **2005**, *15*(10), 1623.

Published on Web 11/30/2009

Recently, Goldenberg et al.[11] introduced new nanocomposites containing functionalized monomers and Au nanoparticles coated with ethyl 11-mercaptoundecanoate that allowed refractive index modulations exceeding 0.007 (i.e., diffraction efficiencies of ca. 50% in 20 μm films) to be achieved. The mechanism of refractive index contrast amplification in this new material was claimed to include both segregation of the components due to photoinduced gradients of concentration and interception of free radicals by Au nanoparticles.

In contrast, and in spite of many works of scientists involved in this field, efforts aimed at fabricating spatially organized metal−polymer nanocomposites by an all-photochemical process were inconclusive and only weak diffraction efficiencies were reported.

We have recently introduced a new procedure that allows metal/polymer nanocomposites to be synthesized from a homogeneous liquid formulation through a photochemically activated sequence of radical reactions. The major innovation lies in the use of visible light to initiate both polymerization of the monomers and reduction of the metal nanoparticles precursor (silver cation) at the same time.[12,13] In short, this mechanism involves (i) the photogeneration of amine-derived initiating radicals ($Amine^{\bullet+}$), (ii) the reduction of silver cations by the aminyl radical produced by the previous reaction, and (iii) the initiation of radical polymerization of the monomer binder.

$$Sens + h\nu \rightarrow Sens^*$$

$$\begin{aligned} Sens^* + Amine &\rightarrow Sens^{\bullet-} + Amine^{\bullet+} \\ Amine^{\bullet+} &\rightarrow Amine^{\bullet} + H^+ \end{aligned} \quad \text{(i)}$$

$$Amine^{\bullet} + Ag^+ \rightarrow X + Ag_0 \quad \text{(ii)}$$

$$Amine^{\bullet} + Monomer \rightarrow Living\ polymer\ radical^{\bullet} \quad \text{(iii)}$$

Following this line on the synthesis of metal/polymer nanocomposites, the present paper discloses preliminary results of an exploratory study devoted to holographic recording with an acrylate formulation containing silver nanoparticles photogenerated in situ.

2. Experimental Section

2.1. Materials. The formulations used in this work contained a liquid acrylic multifunctional monomer (typically, Polyethyleneglycol 400 diacrylate, SR 344 from Sartomer and/or bisphenol A diacrylate, Ebecryl 600 from Cytec). The initiating system was based on a photosensitizer absorbing in the yellow-green range (Eosin Y) and an electron donor (methyldiethanol amin, MDEA, or ethyl dimethyl amino-4-benzoate, EDMAB). These products were purchased from Sigma Aldrich and used as received. The concentration of the sensitizer was adjusted so that the optical density of the samples was ca. 0.6 at maximum (typ. 3×10^{-3} M). The polymerizable formulations were prepared 24 h before use and stored at room temperature in dark conditions.

The precursor of metal nanoparticles was silver nitrate (ACS Reagent 99% from Aldrich). It was added to the formulation as a fine powder and upon stirring, 1 h before use.

2.2. Measurements. Unless otherwise stated, the holographic samples were sandwiched between two glass slides (28×76 mm) separated by a calibrated wedges of 30 μm and kept in close contact by two steel clips. Due to capillary forces, the actual thickness of the samples containing formulations based on SR 344 and E 600 were 23−24 and 45 μm, respectively, depending on the calibrated wedge used.

The absorption spectra were recorded using a Perkin-Elmer Lambda 2 spectrophotometer.

Photochemical reactions were carried out under irradiation at 532 nm with a laser VERDI from Coherent. The progress of the reaction was monitored via UV−vis absorption spectra.

Photopolymerization kinetics was monitored in situ by real-time FTIR with an AVATAR 360 spectrometer from Nicolet. The formulation was sandwiched between two polypropylene films (10 μm thick), deposited on a BaF_2 pellet. Flood exposure during FTIR measurements was performed using a laser diode (type Cube from Coherent) emitting at 532 nm with the average intensity 5 mW/cm^2. The conversion rates are obtained from the disappearance of the progressive vinyl C=C stretching vibration band at 1630 cm^{-1}.

For recording of the holographic gratings, we used a typical setup of four-wave mixing based on a frequency-doubled continuous-wave YAG laser emitting at 532 nm (s-polarization) described earlier.[14] The two arms of the interferometer were equipped with a spatial filter and the fringe visibility could be set with the help of a polarizing beam splitter and a system of half-wave plates. A low-intensity He−Ne laser beam (λ = 633 nm, 0.5 mW) placed at the Bragg angle corresponding to the spatial period of the grating, was used for real-time monitoring of the grating formation. The diffraction efficiency was calculated as $\eta = I_{Diff}/(I_{Tr} + I_{Diff})$ where I_{Tr} and I_{Diff} are the intensities of the first order transmitted and diffracted beams, respectively.

According to the theory of holography, the gratings with spatial period ca. 1 μm and thickness of 16 or 30 μm are Bragg volume gratings [15] ; only 0 and −1 orders were observed in the diffraction pattern.

The angular dependence of the holographic response of the gratings showed excellent agreement with the Kogelnik analysis for thick phase gratings. [16]

A specific device allowed the record to be interrogated by a reading laser diode emitting at 633 nm with incidences covering a ±10° angular window on both sides of the Bragg incidence. The curve showing the actual diffraction efficiency as a function of $\Delta\theta'$ exhibits the well-known squared cardinal sine shape. It was thus possible to use the Kogelnik's relationship for further calculation of the modulation of refractive index (Δn) and the effective thickness of the gratings (d).

The light energy needed for the input and output of the necessary information depends on the efficiency of the holographic recording material. The holographic sensitivity means a

(11) Goldenberg, L. M.; Sakhno, O. V.; Smirnova, T. N.; Helliwell, P.; Chechik, V.; Stumpe, J. *Chem. Mater.* **2008**, *20*(14), 4619 and references therein.
(12) Balan, L.; Jin, M.; Malval, J. P. *Macromolecules* **2008**, *41*(23), 9359.
(13) Balan, L.; Malval, J. P.; Le Nouen, D.; Schneider, R.; Lougnot, D. J. *Polymer* **2009**No. 10.1016/j.polymer.2009.05.003.
(14) Lougnot, D. J.; Turck, C. *Pure Appl. Opt.* **1992**, *1*, 269. Lougnot, D. J.; Turck, C. *Helv. Chim. Acta* **2002**, *85*, 115.
(15) Colier, R. J.; Burckhardt, C. B.; Lin, L. Y.; *Optical Holography*; Academic Press: New York, 1971; p 686.
(16) Kogelnik, H. *Bell Syst. Tech. J.* **1969**, *48*, 2909.

quantity inverse to the input energy (or energy density) at which the necessary output signal level appears.[17] In a way, it measures the build up rate of a hologram. If the visibility is assumed to equal unity, the holographic sensitivity per unit area G (in cm^2/J) expressed as follows[18]

$$G = \eta^{1/2}/I_0 t \quad (1)$$

where I_0 is the power density in the two beams and t is the holographic exposure.

Transmission electron microscopy (TEM) was used to characterize the size and shape of Ag nanoparticules. The sample was cut by means of a microtome (LKB model 8800) and placed onto the copper grid. TEM measurement is carried out using a Philips CM20 instrument with Lab6 cathode. The gratings were examined by atomic force microscopy (AFM) performed using a Pico Plus instrument from Molecular Imaging and a FEI 400 scanning electron microscope (SEM). After disassembly of the samples, the free surfaces of the records were analyzed in tapping mode with a Si_3N_4 tip. The resonance frequency and spring constant of which were 100 kHz and 0.6 N m^{-1}, respectively.

3. Results and Discussion

3.1. Stationary Photolysis. A follow up of the stationary photolysis of the sensitizer/electron donor system was carried out with a view to confirming the initiation process of photopolymerization in the specific formulation used in this work (SR 344, 80%; E 600, 20%; MDEA 0.7 M). Because this system is known to be nonreciprocal in terms of time/intensity equivalence, the fluences used in this experiment were of the same order as those used for holographic recording.

Figure 1 shows the evolution of the UV−visible spectrum of the formulation as the photolysis proceeded. The bleaching of Eosin goes along with the development of a very weak absorption in the blue that finally fades away with the last traces of Eosin. This behavior is consistent with what is reported in the literature.[19] When silver cations are added to this formulation, the bleaching rate of Eosin is about twice as fast and the well-known characteristic absorption band related to the plasmon of silver nanoparticles appears in the blue region. This broadband with a quasi-Gaussian shape has its maximum at 418 nm and a fwhm of ca. 130 nm. It covers the yellow and red part of the spectrum up to 650 nm, a region where Eosin does not absorb at all.

With a view of deriving photophysical parameters from these experiments, we analyzed the photobleaching of Eosin and the corresponding build up of silver nanoparticles quantitatively. The model used considers that the rate of bleaching of the absorbing species ($-dC/dt$) is proportional to the amount of photon absorbed per time and volume unit (I_{abs})

$$-dC/dt = \phi I_{abs} \quad (2)$$

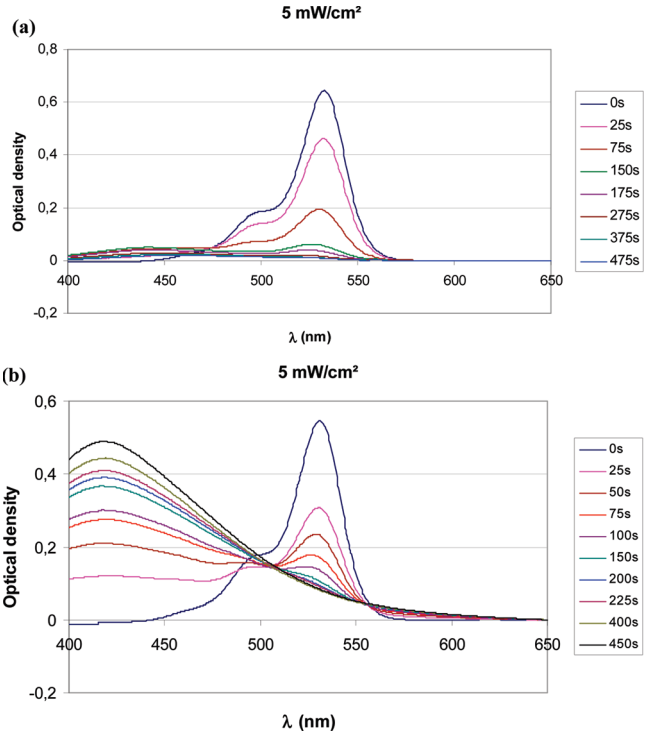

Figure 1. Time evolution of the absorption spectrum of the samples upon irradiation: (a) without silver cations, (b) with silver cations. Fluence: 5 mW/cm^2 at 532 nm.

Details on the integration of this differential equation that is somewhat arduous could be found in the historical papers or reference books dealing with photochemical kinetics.[20] The result arrived at correlates linearly a function of the concentration of the absorbing species that undergoes photobleaching with the exposure:

$$\log[(1/T) - 1] = \varepsilon\phi I_0 t + \log[(1/T_0) - 1] \quad (3)$$

where T and T_0 are the transmission of the sample at time zero and t, respectively, ε is the extinction coefficient of the absorbing species (cm^2.mole), ϕ is the quantum yield of the bleaching process, I_0 is the incident fluence received by the sample (Einstein cm^{-2} s^{-1}), and t is the exposure (s).

As could be expected, the analysis of the experimental data corresponding to the photobleaching of Eosin by MDEA according to this model, leads to a straight correlation of Log $[(1/T) - 1]$ with the exposure t (Figure 2). This result confirms that this process is monophotonic and pseudomonomolecular. Indeed, in the presence of the large concentration of electron donor used (MDEA 0.7 M), all the deactivation pathways of triplet Eosin are negligible with respect to photoreduction.

Quite interestingly, the same kind of treatment applied to the results obtained in the presence of silver cations leads also to a linear correlation, the slope of which is not significantly different from what was observed in the absence of silver. It must be concluded thereof that the reduction mechanism of Eosin remains basically the

(17) Collier, R. J.; Burckhardt, C. B.; Lin, L. H.; *Optical Holography*; Academic Press: New York, 1971.
(18) Carré, C.; Lougnot, D. J. *J. Opt.* **1990**, *21*(3), 147.
(19) (a) Bellin, J. S.; Oster, G. *J. Am. Chem. Soc.* **1957**, *79*(10), 2461. (b) Cohen, S. G.; Parola, A.; Parsons, G. H. *Chem. Rev.* **1973**, *73*(2), 141–161. (c) Valdes-Aguilera, O.; Pathak, C. P.; Shi, J.; Watson, D.; Neckers, D. C. *Macromolecules* **1992**, *25*(2), 541.
(20) Imamura, M.; Koizumi, M.; *Bull. Chem. Soc.* Japan, 1957, *28*(2), 117.

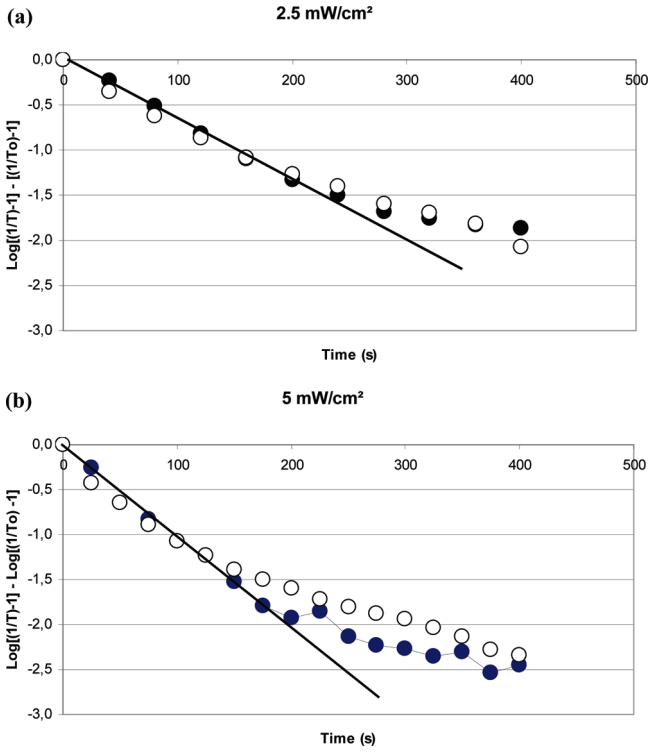

Figure 2. Kinetic analysis of the bleaching of Eosin according to the model of eq 6. Dark circles, without Ag^+; open circles, with Ag^+. (a) 2.5mW/cm^2; (b): 5 mW/cm^2.

same in the presence of silver and the elementary step of reduction of silver cations does not interfere within the primary process of reduction the Eosin sensitizer. Furthermore, the photogenerated species that reduces silver does not regenerate Eosin. And finally, it is worth noticimg that the bleaching rate of the sensitizer is not slowed by the cross-linking polymerization of the liquid monomers that serve as the solvent medium. Assuming the extinction coefficient of Eosin to be 9.2×10^4 at maximum,[21] the quantum yield of photoreduction deduced from the results reported on Figure 1 is $\phi = (6.4 \pm 1.0) \times 10^{-3}$. When the photobleaching was carried out with a fluence of 2.5 mW/cm^2, the same conclusions were arrived at and the quantum yield was observed to slightly decreased to $(6.7 \pm 1.1) \times 10^{-3}$.

These experiments confirm thus, the reduction mechanism of silver cations by aminyl radicals generated through oxidation of a tertiary amine by the photoexcited state of a sensitizer, which was introduced in a previous paper.[12]

3.2. Photocuring in the Absence and in the Presence of Ag^+. The degree of conversion of the samples exposed to the holographic wavelength was evaluated by monitoring the disappearance of the characteristic C=C band of the acrylic group, at 1660 cm^{-1}. At first sight, addition of Ag^+ ions (1 wt % $AgNO_3$) into the liquid formulation does not perturb the polymerization kinetics of the thin film (10 μm) as revealed by the conversion vs time curves reported in Figure 3. On the contrary, the in situ synthesis

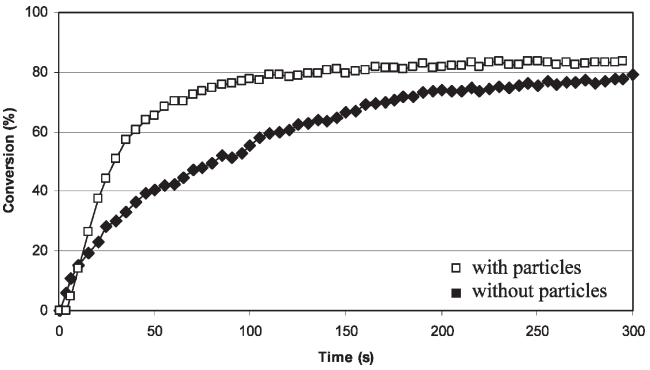

Figure 3. Influence of silver nanoparticles on the conversion of SR 344 double bonds upon irradiation at 532 nm and at room temperature. Thickness = 10 μm, light intensity = 3.5 mW/cm^2.

of silver nanoparticles concomitantly with the photopolymerization process was observed to have an unexpectedly favorable effect on the rate of polymerization (R_p) (for instance, after a 100 s-exposure, the conversion ratio are 55 and 80% in the absence and presence of nanoparticles, respectively).

The formation of silver nanoparticules during polymerization was revealed by the progressive change of color of the sample that turned from light purple (Eosine) to brown-yellow (silver nanoparticles). The UV−vis spectrum (Figure 1b) showed a maximum absorption at ca. 418 nm that is associated with the surface plasmon resonance of silver nanoparticules.[22]

As can be observed in Figure 3, the development of silver nanoparticles in the formulation has a 3-fold influence on the polymerization kinetics. In the presence of metal nanoparticles, the polymerization started after a short inhibition period (ca. 5 s), the conversion leveled off at a slightly higher value (83% instead of 75%) and above all, the R_p was accelerated by a factor of 1.9 (in the presence of MNPs, R_p is 2.6 M L^{-1} s^{-1} and without particles 1.4 M L^{-1} s^{-1}).

*R*p is defined as the maximum of the first derivative of the conversion vs time curves. This corresponds to the early time of the polymerization and the monomer concentration was taken as the initial bulk concentration ($[M]_0$).

3.4. Characterization of the Silver Nanoparticles Generated In situ. Figure 4a shows a TEM image of a sample with [BC] = 0.2 M, [Ag^+] = 0.5% w/w irradiated with a fluence of 10 mW/cm^2 for 60 s. Spherical nanoparticules are clearly visible with an average diameter of 5 ± 0.3 nm. The particle size distribution (Figure 4b) was evaluated from the analysis of this TEM image on a collection of 500 particles. This image confirms the absence of aggregation of the nanoparticles.

3.5. Holographic Recording. A formulation containing SR 344 (80%) and E 600 (20%), which is capable of generating silver nanoparticles in situ, was used to record holographic gratings. An example of holographic sensitivity

(21) Pauporté, T.; Yoshida, T.; Goux, A.; Lincot, D. *J. Electroanal. Chem.* **2002**, *534*(1), 55.

(22) (a) He, R.; Qian, X.; Yin, J.; Zhu, Z. *J. Mater. Chem.* **2002**, *12*, 3783. (b) Xie, Y.; Ye, R.; Liu, H. *Colloids Surf., A* **2006**, *279*, 175. (c) Balan, L.; Malval, J. P.; Schneider, R.; Burget, D. *Mater. Chem. Phys.* **2007**, *104*(2−3), 417.

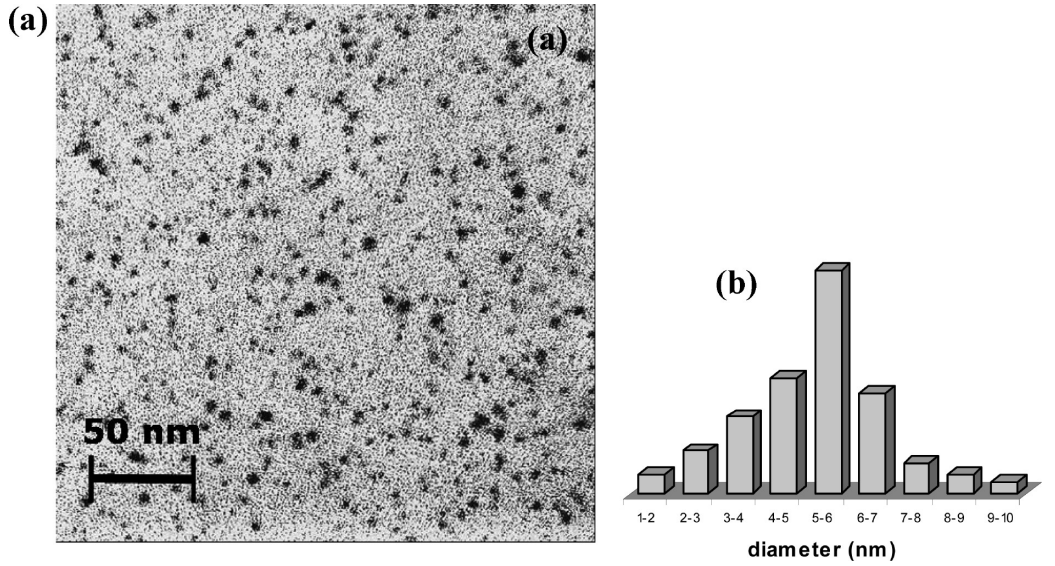

Figure 4. (a) Bright-field TEM micrograph and (b) the corresponding particle size distribution of silver nanoparticles.

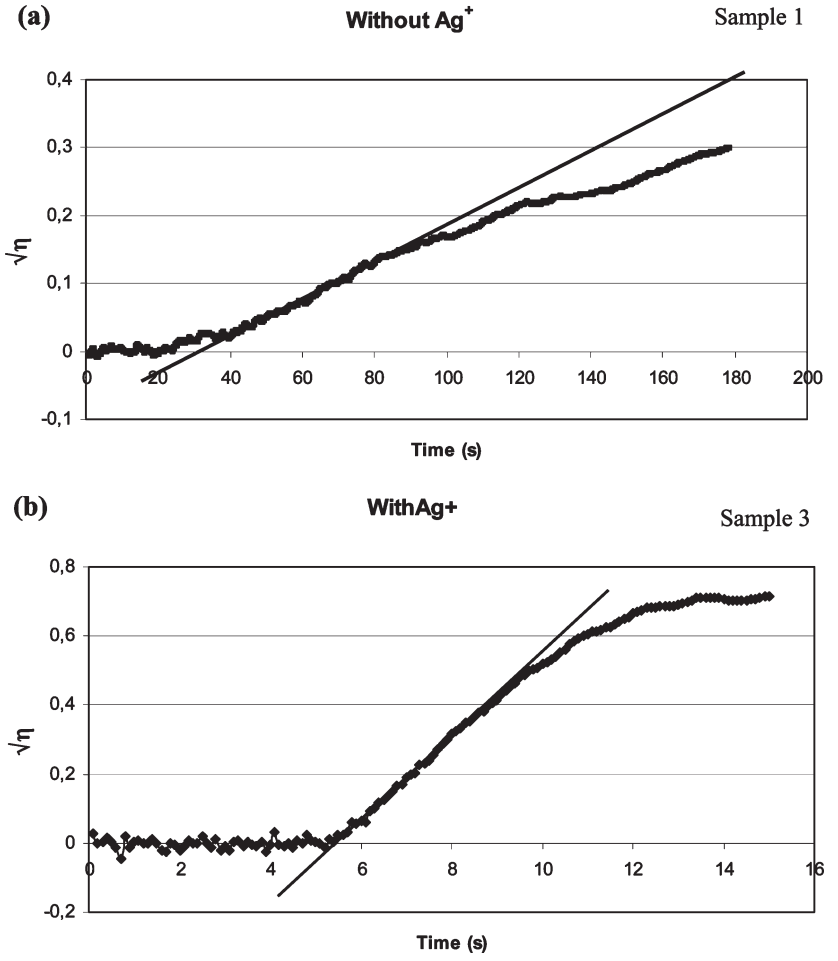

Figure 5. Holographic sensitivity curve derived from holographic recording results of (a) sample 1 without Ag^+ and (b) sample 3 with 1% w/w Ag^+ in Table 1 with the model of eq 4.

curves without and with silver nanoparticles is shown in Figure 5. The holographic sensitivity and efficiency at maximum of the gratings and the refractive index modulation achieved are presented in table 1 as a function of the recording conditions.

As can be seen from these results, the reference system was deliberately selected because of its poor recording performances. It is characterized by a limited potential in terms of available index modulation that is related to the use of a mixture of two acrylic difunctional monomers

Table 1. Influence of the Chemical and Photonic Parameters on the Holographic Sensitivity, Diffraction Efficiency at Maximum of the Gratings, and Refractive Index Modulation

sample	EDMAB (M)	Ag^+ (% w/w)[a]	total fluence (mW/cm^2)	exposure (s)	η_{max} (%)	Δn ($\times 10^{-5}$)	G (cm^2/J)
1	0.4	0	20.8	180	8.9	121	0.13
2	0.4	0	41.8	240	16.9	185	0.12
3	0.4	1	10.0	60	52.7	290	12.2
4	0.4	1	10.0	15	41.1	265	12.3
5	0.2	0.5	5.0	150	68.1	308	4.2
6	0.2	0.5	10.0	100	69.2	303	3.9
7	0.2	0.5	20.0	60	80.0	376	2.8
8	0.2	1	10.0	60	48.7	300	4.8
9	0.2	1	20.0	30	72.5	329	3.6

[a] 0.5% w/w = 0.024 M; 1% w/w = 0.059 M.

and a tertiary amine generating EDAB-derived aminyl radicals that are reputedly mediocre initiators of polymerization.[23] In such a formulation, the fate of silver nanoparticles is to undergo spatial segregation under the influence of driving forces resulting from differences of local properties between dark and bright fringes. Among the possible causes for this segregation, one can mention gradients of photoreduction rate of silver cations or gradients of cross-linking degree of the monomers, that both replicate the spatial distribution of the actinic light in the incident interference pattern.

The recording characteristics of the formulation containing silver cations appeared to be deeply changed. The amplitude of the available modulation of refractive index is much larger while the holographic sensitivity increases up to a hundredfold with $[Ag^+]$ = 1% w/w. There is no doubt that the presence of silver nanoparticles photogenerated in situ is the key factor that is behind the dramatic improvement of the recording properties. However, it is worth of notice that a 2-fold increase of the concentration in silver cations did not drastically change the recording process: the holographic efficiency increased by some 20%, whereas η_{max} decreased slightly.

The results reported in Table 1 also reveal the influence of both the chemical and photonic parameters on the diffraction efficiency at maximum and the holographic efficiency. In the presence of silver, addition of increasing the amount of co-initiator (EDMAB) results in an important acceleration of the recording process. This observation is mainly accounted for by the increase of the photoreduction quantum yield of Eosin (ϕ) in its triplet state by EDMAB.[24]

$$\phi = k_{PR}[\text{Eos}^*][\text{BC}]/(k_D + k_{PR}[\text{Eos}^*][\text{BC}]) \quad (4)$$

with k_{PR}: rate constant of the electron transfer between triplet Eosin and EDMAB, and k_D: rate constant of the deactivation of Eosin to ground state.

Table 1 shows also that increasing the holographic recording fluence always goes along with an increase of the diffraction efficiency at maximum but also with a decrease of the holographic efficiency. This behavior is to be interpreted in terms of coupling between chemical reactions generating active species involved in the modulation of refractive index and physical processes responsible for the segregation of the components of the holographic formulation. The higher the fluence used to record the holographic grating, the faster the recording process but the less efficient is the segregation process.[25]

Since the concentrations of Ag+ used in this work are quite small, the increase of refractive index modulation cannot be only accounted for by the presence of silver nanoparticles. Clearly, indirect physical and chemical effects of the nanoparticles must be invoked. Because of their strong interaction with nucleophilic groups, they are able to modify the polymerization kinetics and as an indirect consequence, the composition and morphology of the copolymer formed at the local scale. Given the difference of chemical structure and refractive index between the comonomers used (n_{E600} = 1.548 and n_{SR344} = 1.466), only a 1%-modification of the copolymer composition between bright and dark areas of the record induces an increase of refractive index modulation of ca. 150×10^{-5}.

3.6. Analysis of the Records by AFM. Figure 6 shows the AFM characterization of two samples obtained with formulations without particles and with 1% w/w Ag^+, respectively. The samples were disassembled before analysis and the free surface was kept for 24 h under vacuum to obtain a complete release of constraints stored in the polymer matrix.

Figure 6a−c show the microstructures obtained at the surface of the sample containing no Ag^0. On the topographic image (Figure 6 a), the grating can be clearly observed. The amplitude of the relief is ca. 50 nm (Figure 6 c). This surface corrugation results from the difference in the polymer structure between the bright and dark areas of the incident interference pattern. Such a surface corrugation was already observed in other photopolymerizable systems.[26] The period measured by AFM corresponds exactly to the period of the interference pattern (1 μm).

In the case of Ag-doped material (Figure 6 d−f), the grating was also clearly visible. The relief of the surface corrugation is of the same order as observed in the sample without NPs, thus demonstrating that the polymer matrix is not significantly affected by the presence of silver NPs generated in situ. The contrast in the phase image is directly linked to difference in the polymer material structure. In the case of the Ag-doped system, this contrast is more pronounced, meaning that the addition of Ag^+ favors the appearance of gradients in the polymer structure. This observation is in agreement with the higher diffraction efficiency linked to the addition of Ag^+. A close examination of the topography reveals a higher surface roughness in the case of the Ag-doped sample. The protuberances appearing in the phase image correspond to bright dots (Figure 6e); without hesitation, they can be attributed to silver NPs because the mechanical

(23) Pyszka, I.; Kucybała, Z. *Polym. Bull.* **2008**, *61*, 553.
(24) Noiret, N.; Meyer, C.; Lougnot, D. J. *Pure Appl. Opt.* **1994**, *3*, 55.
(25) Samui, A. B. *Recent Pat. Mater. Sci.* **2008**, *1*, 74.
(26) Jradi, S.; Soppera, O.; Lougnot, D. J. *J. Microsc.* **2008**, *229*, 151.

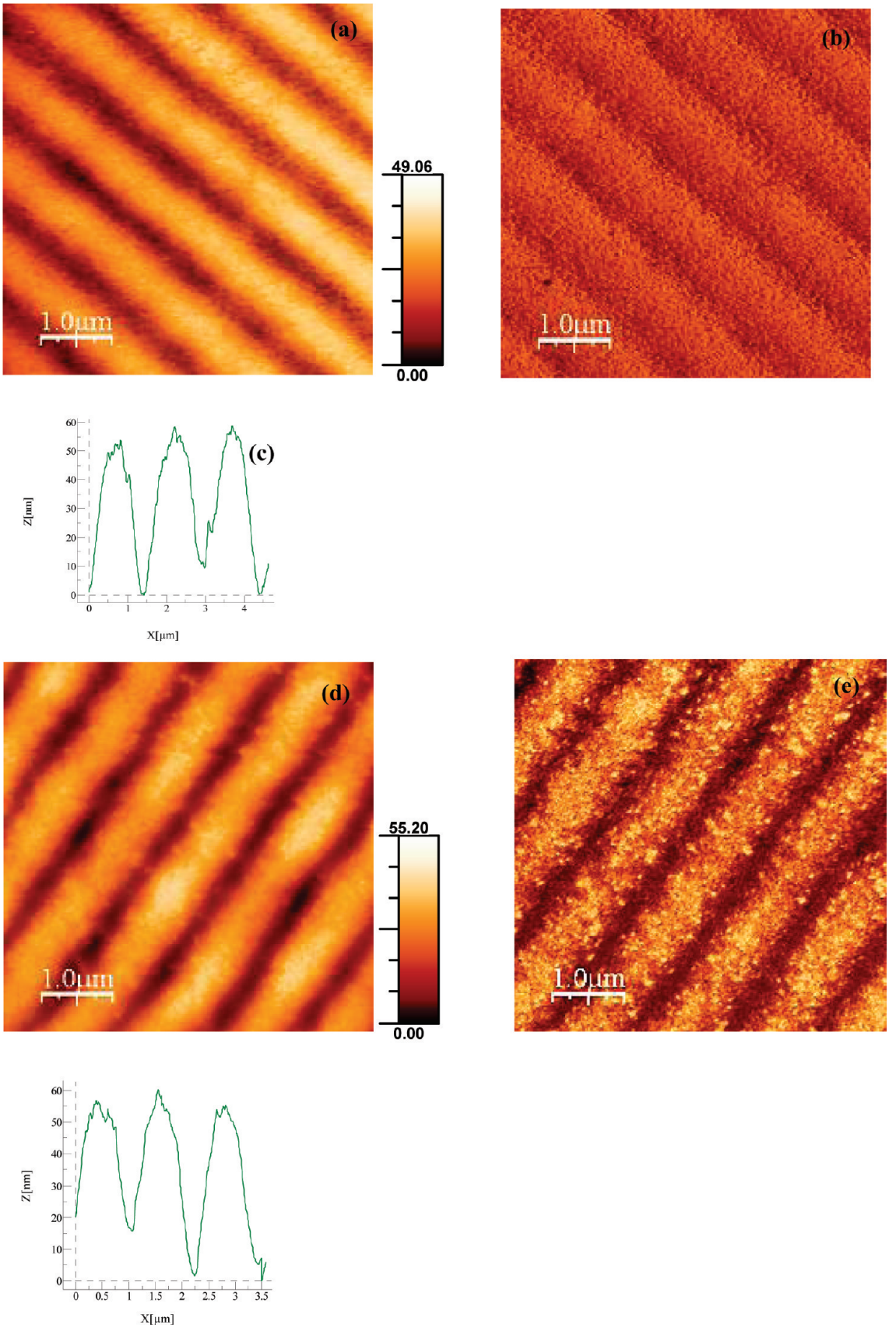

Figure 6. AFM images obtained in tapping mode of holographic records without and with silver cations: (a) topography, (b) phase, and (c) cross-section without Ag^+; (d) topography, (e) phase, and (f) cross-section with Ag^+.

interaction between the AFM tip and the MNP emerging from the polymer surface is different than response on metal. Interestingly, NPs are not distributed homogeneously over the surface of the sample: Ag NPs accumulate in

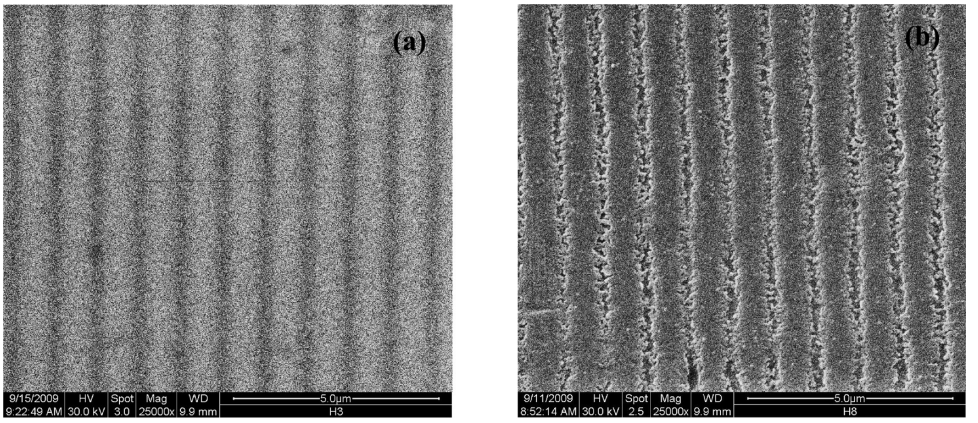

Figure 7. SEM images of holographic records (a) without and (b) with 1% silver cations.

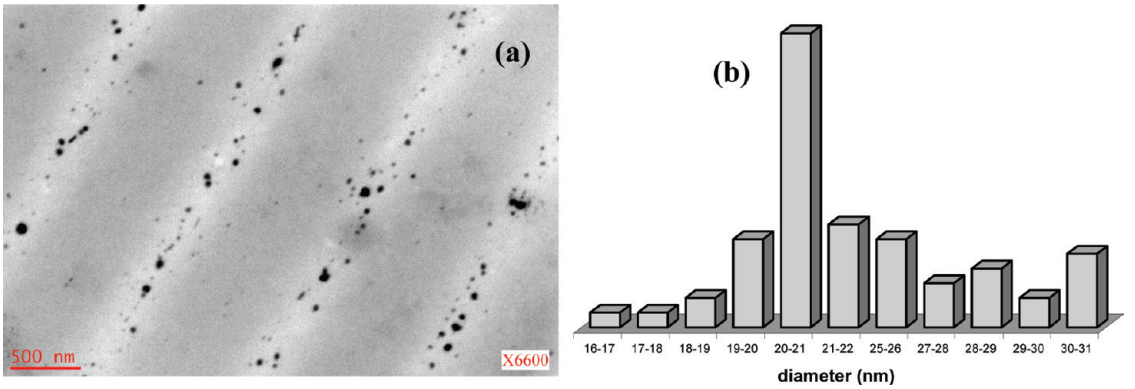

Figure 8. (a) TEM micrograph of the grating formed with silver nanoparticles and (b) the distribution of the diameter of silver nanoparticles.

the protruding regions of the grating. This spatial segregation is the key-factor accounting for the increase of holographic efficiency observed in doped samples.

Figure 7 shows the micrographs recorded by scanning electron microscope (SEM) of two UV-cured samples obtained with Ag^+ and without Ag^+ respectively. Clearly, silver NPs induce physical changes in the polymer (morphology, free volume) and chemical changes (local composition of the copolymer formed in the presence of nanoparticules.[27] Presumably, the refractive change results not only from the segregation of the nanoparticles but also from the important change in the structure of the polymer.

The TEM image (Figure 8a) confirms without contest a patterned distribution of individual nanoparticles in the polymer matrix that form a grating with a period of ca. 1 μm. As can be seen, the size of the spherical NPs ranges from 15 to 30 nm, with an average diameter of ca. 21 nm (Figure 8b).

4. Conclusion

Only very few examples of metal nanoparticle manipulation by photochemical processes were reported up to now, and most of them used dispersions of dry nanoparticles in a liquid formulation. In another respect, photoassisted processes allowing the generation of polymer/metal nanocomposites that were introduced very recently are still in demand of further investigation.

The present paper introduces an innovative approach combining these two ideas. It reports on the use of a photopolymerizable formulation that is capable of generating metal nanoparticles in situ to record holographic gratings. The process used avoids handling dry metal NPs and aggregation that takes place during dispersion in a liquid formulation.

Quite interestingly, the presence of metal NPs was observed to accelerate and improve the cross-linking of multifunctional monomers forming the continuous recording medium, whereas the quantum yield of photobleaching of the sensitizer involved in the initiation process remained unaffected. And finally, AFM and TEM analysis of the holographic gratings recorded with this formulation revealed an accumulation of NPs that is directly related to the dramatic improvement of the recording characteristics of the formulation when NP precursor is present.

Obviously, the holographic efficiency of the photochemically assisted process depends on the efficiency of the coupling between the reaction generating NPs and the photocuring of the polymerizable formulation.

This process provides a robust way to manipulate NPs at the nanoscale and offers a means to fabricate microoptical elements, the design of which involves a patterning of the spatial distribution of NPs. It should open new vistas in the field of microoptics and plasmonics.

Acknowledgment. The authors thank the Agence Nationale pour la Recherche (ANR), under grant PHOTOHYBRID (BLANC 07-26188654).

(27) Yagci, Y; Sangermano, M; Rizza, G. *Chem. Commun.* **2008**, *24*, 2771.